# Noncontact Extraction of Biomechanical Parameters in Gait Analysis Using a Multi-Input and Multi-Output Radar Sensor

**DINGYANG WANG**[1], (Student Member, IEEE), **JUNYOUNG PARK**[1], (Student Member, IEEE), **HEE-JIN KIM**[2], **KOUNSEOK LEE**[3], AND **SUNG HO CHO**[1], (Member, IEEE)

[1]Department of Electronic Engineering, Hanyang University, Seoul 04763, South Korea
[2]Department of Neurology, College of Medicine, Hanyang University, Seoul 04763, South Korea
[3]Department of Psychiatry, College of Medicine, Hanyang University, Seoul 04763, South Korea

Corresponding author: Sung Ho Cho (dragon@hanyang.ac.kr)

**ABSTRACT** Gait analysis is one of the most basic methods for assessing a patient's biopsychological status. Doctors can distinguish people with mental and neurological disorders by monitoring their gait. To perform gait analysis in a more quantitative and accurate manner, many studies have used inertial measurement units (IMUs), cameras and ground reaction force platforms. However, conventional gait analysis requires sensors to be attached to the subject's body, and some of them are cost prohibitive. Currently, studies of noncontact gait analysis using radar sensors are being performed. Such studies have successfully measured several gait parameters associated with the noncontact method but have been unable to distinguish between individual legs. In this study, we proposed a method for noncontact gait analysis with a treadmill that could separate the left and right legs using multi-input and multi-output frequency-modulated continuous-wave (MIMO FMCW) radar. By recognizing two legs in a range-Doppler map and estimating their angles, ranges and velocities, the gait parameters of the individual legs could be identified. We performed experiments with 15 participants in 4 scenarios (walking, running, left leg limping, right leg limping) and compared gait parameters obtained using FMCW radar and IMUs. The gait parameter measurements were validated using the intraclass correlation value, and they showed excellent agreement except for flight time. Moreover, a parameter was identified that can accurately detect gait asymmetry, and its sensitivity (0.83) and specificity (1.00) were validated. Our future research will analyze not only feet movement but also arm movement so that it can be further applied to the medical field.

**INDEX TERMS** Ambient-assisted living, gait analysis, gait asymmetry, individual leg perception, MIMO FMCW radar.

## I. INTRODUCTION

Gait analysis encompasses the measurement and assessment of quantities that represent human motion characteristics. Several fields, including orthopedics, rheumatism, neurology, and rehabilitation, have investigated the relationship between human walking styles and symptoms of diseases, such as frailty and dementia. In particular, many pathological diseases cause differences in left and right leg movements,

The associate editor coordinating the review of this manuscript and approving it for publication was Zihuai Lin.

which is known as gait asymmetry [1]. Early detection of gait asymmetry can aid in early diagnosis, facilitating proper treatment and improved prognosis.

Recently, many types of sensors have been studied and applied to gait analysis, one of which is an inertial measurement unit (IMU) sensor [2], [3]. IMU sensor-based gait analysis systems have been proposed for continuous monitoring of a person's gait and foot trajectory [4] during daily life activities. An IMU sensor-based body alignment method [5] can monitor the joint angles of the lower limb, but there are limitations to measuring a fast gait. IMU sensors are also

used for assisted sensing in gait rehabilitation [6]. Most of the sensors usually need to be attached to the body. Unlike non-contact sensors that can observe movement from a distance without any interference, it is inconvenient and can cause discomfort to the user. There have been several studies using noncontact sensors, such as RGB cameras, depth cameras and radar. RGB camera-based gait analysis [7] demonstrates the classification of normal and abnormal human gaits. In [8], image-based physical features were extracted, and small differences could be detected between the step motions, which resulted in gait asymmetry. The four subjects with different diagnosed gait disorders participated in the experiment and showed that gait asymmetry could be detected with high accuracy. However, in that study, data had to be collected, classified, and processed offline before use. In addition, the system could not differentiate between the left and right feet. In [9], a depth camera was used to evaluate gait symmetry with mirrors, but the experimental environment was too complex to construct. Most importantly, cameras can compromise privacy and are susceptible to ambient light. Table. 1 shows the most commonly used or studied gait sensors and evaluates them based on several items. Because of the many advantages that radar sensors have, interest in radar has increased, and there have been many studies, including people counting [10], vital sign monitoring [11], [12], gesture recognition [13], [14] and movement quantification [15], using radar.

**TABLE 1.** Qualitative comparison of gait sensors.

| | Motion capture camera | Treadmill with built-in ground reaction force | IMU sensor | FMCW radar |
|---|---|---|---|---|
| Cost | High | High | Low | Low |
| Non-contact | o | x | x | o |
| Continuous measurement | o | o | o | o |
| Individual foot distinction | o | o | o | o |
| Privacy issue | o | x | x | x |
| Convenience of use | x | o | o | o |
| Computing load | High | Medium | Low | Medium |

Previous studies involving radar include the identification of gait-motion characteristics of subjects and the classification of different arm motions [16]. In [17], the authors demonstrated the possibility of using Doppler radar to extract medically relevant parameters, such as stride rate and walking velocity, to characterize a subject's gait. In [18] and [19], the authors aimed to identify subjects and classify gait according to an individual's walking styles using a machine learning technique. Data measured using radar can provide more quantitative diagnostic evidence than a doctor's visual diagnosis, thus reducing intra- and interobserver variability and the likelihood of human error in gait analysis.

Even though radar has been applied to noncontact gait analysis in a concise and low-cost manner, previous studies

could not provide gait parameters for the left and right feet separately with high accuracy. In the medical field, it is important to obtain detailed gait parameters to analyze a patient's symptoms. In [20], older women with knee extensor strength asymmetry were found to experience gait asymmetry, leading to a high probability of falling, which can be detrimental. In older adults, gait asymmetry is proven to be relevant to fall risk, and their daily living quality can be affected [21]. Prosthetics users who exhibit unnatural gait patterns have been shown to require more effort to compensate for their unwanted motions [22]. Moreover, in [23], Parkinson's disease and elderly fallers showed a great level of gait asymmetry during the natural walking condition compared with the control group. Especially for older people, it is important to monitor gait separation of the left and right feet.

In this paper, a quantitative gait analysis on a treadmill that can separate the left and right foot using multi-input and multi-output (MIMO) frequency-modulated continuous-wave (FMCW) radar is proposed. FMCW radar was developed based on Doppler radar and can measure range and velocity accurately. The IMU sensors are used as a reference sensor to compare the agreement of the radar measurements. IMU sensor-based motion capture methods have previously been utilized for human motion capture [24]. In [25], the authors showed an IMU sensor for indoor position estimation. The experiment was performed with 15 participants in 4 scenarios. In the scenarios, participants were asked to walk and run on a treadmill, and they were then asked to walk on a treadmill with knee flexion and wearing a knee orthosis, which limited the walking motion, to simulate an abnormal gait. The gait parameters, such as stride time, stance time, flight time, step time, maximum foot velocity interval and cadence, were measured from the left and right legs separately, and the agreement between the FMCW radar and IMU sensor was compared (Fig. 1). Moreover, gait asymmetry was detected using some of the gait parameters measured with FMCW radar.
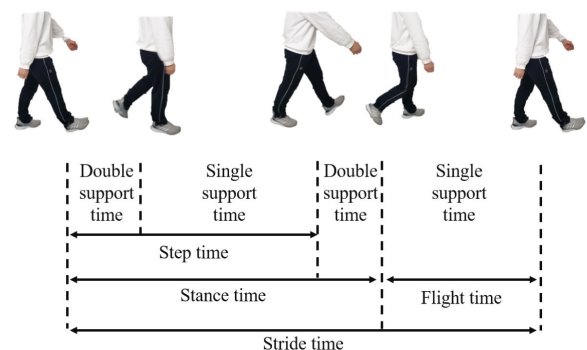


**FIGURE 1.** Example of gait parameter definition.

This paper is organized as follows: Section II describes background information on FMCW radar, including the signal model and basic signal processing. Section III

introduces the algorithm that recognizes the left and right feet and extracts gait parameters. Section IV describes the experimental environment, including the sensor setup, baseline information, experimental protocol and statistical analysis. Section V shows the statistical results, including agreement between the FMCW radar and IMU sensor, and the numerical results, including gait asymmetry detection. Finally, Section VI draws conclusions and describes future research.

## II. BACKGROUND

### A. FMCW RADAR SIGNAL MODEL

The FMCW signal transmitted in the time domain can be defined as [26]:

$$x_0(t) = \exp\left(j2\pi\left(f_c t + \frac{\mu}{2}t^2\right)\right) \quad (1)$$

where $f_c$ is the carrier frequency, $\mu$ is the rate of change (slope) of the instantaneous frequency of a chirp signal ($\mu = f_{BW}/T_c$), $f_{BW}$ is the bandwidth of the chirp signal, and $T_c$ is the sweep time of a chirp signal. In an FMCW signal frame, the number of chirps can be multiple, and the total length of $L$ chirps is defined as:

$$x(t) = \sum_{l=0}^{L-1} x_0(t) \, Rect \, (t - lT_c) \quad (2)$$

where $l$ is the count of the $l$th chirp in a frame and $Rect(t)$ is the normalized rectangular function. $x(t)$ is the total length of $L$ chirps in a data frame.

Consider $M$ targets impinging on a uniform linear array of a total of $K$ antenna elements. The received signal of the $k$th antenna of the $l$th chirp is denoted by $r_{l,k}(t)$ and is expressed as:

$$r_{l,k}(t) = \sum_{m=1}^{M} A_m x_0(t - \tau_m) \exp\left(j2\pi\left(f_{d,m}T_c l\right)\right)$$
$$\times \exp\left(j\frac{2\pi}{\lambda}sk\sin\theta_m\right) + N_{l,k}$$
$$\text{for k} = 1, \ldots, K \quad (3)$$

where $A_m$ is the complex amplitude of the $m$th target, $\tau_m$ is the round-trip delay corresponding to the range of the $m$th target, $f_{d,m}$ is the Doppler frequency of the $m$th moving target, $s$ is the spacing between adjacent antennas, $\theta_m$ denotes the DOA of the $m$th target, and $N_{l,k}$ is the additive white Gaussian noise (AWGN) at the $k$th antenna and $l$th chirp. In the receiving part, the dechirping process is defined as the multiplication of the received FMCW signal $r_{l,k}(t)$ and the conjugation of the transmitted chirp signal $x_0^*(t)$. Here, $s$ is assumed to be $s = \lambda/2$, where $\lambda$ is the wavelength of the carrier frequency. $\tilde{A}_m$ is the amplitude of the $m$th target, $R_m(t)$ is the time of arrival (TOA) term, and $v_m^l$ and $z_m^k$ are the Doppler term and direction of arrival (DOA) term, respectively. $\tilde{N}_{l,k}(t)$ is the receiving

noise term.

$$y_{l,k}(t) = r_{l,k}(t)x_0^*(t)$$
$$= \sum_{m=1}^{M} A_m \exp(-j2\pi(f_c\tau_m - \mu\tau_m^2/2$$
$$+ \mu\tau_m t - f_{d,m}Tl - k\sin\theta_m/2)) + N_{l,k}x_0^*(t)$$
$$= \sum_{m=1}^{M} \tilde{A}_m R_m(t)v_m^l z_m^k + \tilde{N}_{l,k}(t) \quad (4)$$

### B. BASIC SIGNAL PROCESSING

The received signal passes to the analog-to-digital converter (ADC), and equation (4) can be converted into the discrete time equation, which is denoted by $y_{l,k}[n]$, where $y_{l,k}[n] = y_{l,k}(nT_s)$ for $n = 0, 1, \ldots N-1$, and $T_s = 1/f_s$ with the ADC sampling frequency $f_s$. The $y_{l,k}(t)$ can be rewritten as:

$$y_{l,k}[n] = \sum_{m=1}^{M} \tilde{A}_m R_m[n]v_m^l z_m^k + \tilde{N}_{l,k}[n] \quad (5)$$

As shown in Fig. 2, the TOA term $R_m[n]$ can be used to estimate the range of the target using a 1D discrete Fourier transform (DFT) for each chirp. The Doppler term $v_m^l$ can be used to estimate the velocity of a moving target using 1D-DFT for chirps in a frame. Some 2D-DFTs are used to estimate the range and velocity at once [27].

The figure below the block labeled 'Velocity Estimation' in Fig. 2 describes the range-velocity map after applying 2D-DFT to a received radar frame. The blue color in the figure indicates that the value is small, meaning noise or clutter, and the yellow color indicates the moving target. Subsequently, peaks can be found in the range-velocity map to estimate the DOA, corresponding to the block labeled 'Find Peaks' in Fig. 2. The blue triangles in the red dotted box indicate the peaks detected using the MATLAB built-in function (*findpeaks*) [28].

To estimate the DOA of the detected peaks of moving targets, DFT was applied. In the DOA estimation process, the TOA and Doppler terms can be expressed as a new variable $G_m$, where $G_m = \tilde{A}_m R_m[n]v_m^l$, and $y_{l,k}[n]$ can be rewritten as $\gamma_{k,m}$ for the $m$th peak at the $k$th antenna; (5) is simply expressed as follows:

$$\gamma_{k,m} = G_m z_m^k + \hat{N}_k \quad (6)$$

The $i$th $K$ point DFT output of $\gamma_{k,m}$ is denoted by $\psi_{i,m}$

$$\psi_{i,m} = \sum_{k=1}^{K} \gamma_{k,m} \exp\left(\frac{-j2\pi}{K}i(k-1)\right) \quad \text{for i} = 1, 2, \ldots K \quad (7)$$

where $K$ is the number of receiving antenna elements and $\psi_{i,m}$ is the $i$th-point DFT result calculated from the $m$th peak in a frame range-velocity map. Before making the angle estimation, Doppler compensation was performed due to the use of time-division multiplexing (TDM) MIMO, which is described in detail in the Sensor Setup part of Section IV.
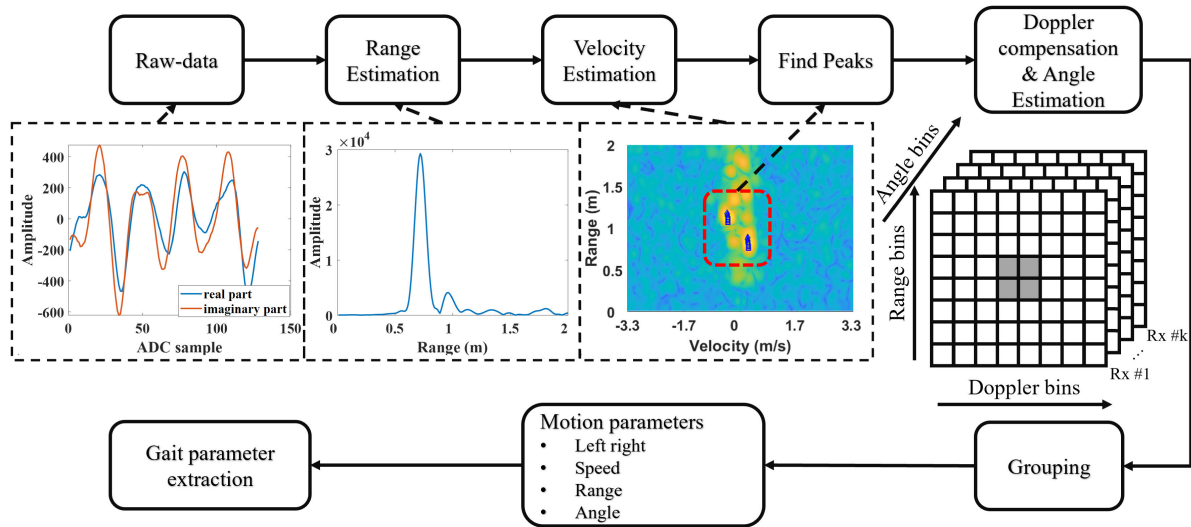
**FIGURE 2.** Flow diagram of extracting gait parameters from FMCW raw data.

To estimate the angle, the peak detection processing for the DFT result is performed, i.e., $ang_m$ is the peak index of the DFT result, corresponding to $M$ peaks in $\psi_{i,m}$, and is obtained for $m = 1, \ldots, M$; here, $M = 25$ assuming enough peaks of the left and right foot were detected.

## III. METHODS

As shown in Fig. 2, this section describes the method of identifying the left and right foot after extracting the peaks from the range-velocity map. The method extracts medical gait parameters from the range, velocity, and angle motion trajectory data.

### A. LEFT OR RIGHT LOWER LIMB RECOGNITION AND NOISE SUPPRESSION USING A DYNAMIC MODEL

Before grouping the total $M$ peaks from the range-velocity map, we rewrite the Doppler (velocity) and TOA (range) terms as $vel_m$ and $dis_m$, respectively. $P_m$ is the set of range, velocity and angle information of the $m$th peak.

$$P_m = \{vel_m, dis_m, ang_m\} \quad \text{for m = 1 : M} \quad (8)$$

where $M$ is the total number of peaks detected in the range-velocity map.

Clustering is a useful tool for finding structures in data sets, and the mixed likelihood method is a popular clustering method, of which the expectation-maximization (EM) algorithm is the most commonly used method. The EM algorithm is an iterative approach that cycles between two steps. The first step is to estimate the missing variables, called the E-step. The second step attempts to optimize the parameters of the model to best explain the data, called the M-step. In one study, [29] developed an algorithm that is suitable for clustering high-dimensional data in an accurate and time-efficient manner. In [30], the author developed a robust EM clustering

algorithm that can solve the initialization problem and automatically obtain the number of clusters.

In this work, the previously extracted data set has range, velocity and angle features. To identify whether these data are from the left or right foot, we need to group the data according to the features. Assuming the detected peaks $P_m$ in (8) are all from the moving targets, the grouping number $g$ is set to 2, corresponding to the left and right foot groups.

The peak data set $\{P_1, P_2, \ldots P_m\}$ is detected from the range-velocity map with size $m$. Three features can be considered as a mixture model for $g = 2$ clusters. The peak data could be from the $d$-variate Gaussian mixture model

$$\begin{aligned} f(p; \alpha, \theta) &= \sum_{k=1}^{g} \alpha_k f(p; \theta_k) \\ &= \sum_{k=1}^{g} \frac{\alpha_k}{\sqrt{|\Sigma_k|(2\pi)^d}} \\ &\quad \times \exp\left(-\frac{1}{2}(p - \mu_k)\Sigma_k^{-1}(p - \mu_k)^T\right) \quad (9) \end{aligned}$$

where $\alpha_k > 0$ denotes the mixing proportions with the constraint $\sum_{k=1}^{g} \alpha_k = 1$ and $f(p; \theta_k)$ denotes the density of $p$ from the $k$th cluster with corresponding parameters $\theta_k$; here, $\theta_k$ is the mean vector ($\mu_k$) and covariance matrix ($\Sigma_k$) of the distribution.

E-step: $z_{km}$ is the missing value for each cluster and is unknown; the conditional expected value of $E(Z_{km}|p_i; \alpha, \theta)$ is substituted for $z_{km}$.

$$\hat{z}_{km} = E(Z_{km}|p_i; \alpha, \theta) = \frac{\alpha_k f(p_m; \theta_k)}{\sum_{s=1}^{g} \alpha_k f(p_m; \theta_k)} \quad (10)$$

where $\hat{z}_{km}$ indicates the expectation value belonging to each cluster.

M-step: under the constraint $\sum_{k=1}^{C} \alpha_k = 1$, to maximize

$$\hat{L}(\alpha, \theta; x_1, \ldots x_n) = \sum_{i=1}^{n} \sum_{k=1}^{C} \hat{z}_{km} ln[\alpha_k f(x_m; \theta_k)] \quad (11)$$

The parameter $\theta_k$ consists of a mean vector and a covariance matrix, and the update equations are as follows:

$$\mu_k = \frac{\sum_{m=1}^{M} \hat{z}_{km} x_m}{\sum_{m=1}^{M} \hat{z}_{km}} \quad (12)$$

$$\Sigma_k = \frac{\sum_{m=1}^{M} \hat{z}_{km} (x_m - \mu_k)(x_m - \mu_k)^T}{\sum_{m=1}^{M} \hat{z}_{km}} \quad (13)$$

The update equation for mixing proportions is expressed by

$$\alpha_k = \frac{\sum_{m=1}^{M} \hat{z}_{km}}{M} \quad (14)$$

The stop condition is when $\|\mu_k^{(s+1)} - \mu_k^{(s)}\| < \varepsilon$ is satisfied; otherwise, the E-step, M-step and $s = s + 1$ are run. $\varepsilon$ is the stop threshold, and $s$ is the iteration number starting from 1. Finally, the group information is obtained from

$$G_m = \begin{cases} 1 & \text{if } z_{\hat{1},m} \geq z_{\hat{2},m} \\ 0 & \text{if } z_{\hat{1},m} < z_{\hat{2},m}. \end{cases}$$

Once the group information is obtained, we compare the angle information of each group and determine the left and right groups. This is possible because the detected peaks from the left foot and right foot have different DOAs. The peaks of the left and right feet after grouping are shown in Fig. 3. The point closest to the center point in each group is used as the motion parameter for the current data frame.
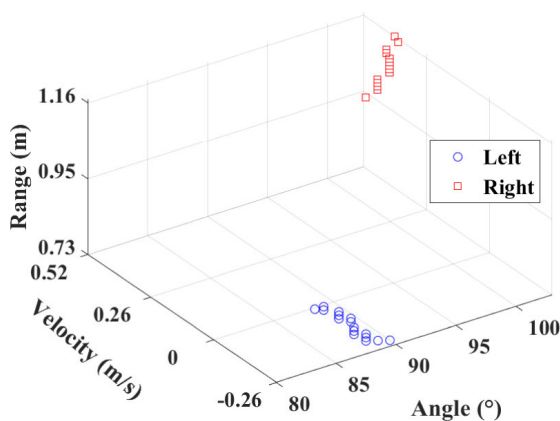


**FIGURE 3.** Example of grouping and separating the left and right feet according to range, velocity and angle measurements from FMCW radar.

In the ideal case, the peaks are only from the left or right foot. However, in actual experiments, the moving targets also come from the knee and leg, which may lead to false detection. Before the grouping process, we have the range, velocity and angle data; however, we do not know the left or right

foot information, so we cannot perform the noise reduction algorithm on nonsequential data. Once the data are grouped into left and right feet, the peaks can be linked sequentially by the group information on the time axis. Then, the Kalman filter [31] can be performed separately for each group of sequential data. In this part, we use the dynamic motion model to estimate the a priori parameters (state parameters and covariance matrix) in the prediction phase. In the update phase, the improved a posteriori state is estimated by the residual difference between the currently predicted and currently observed data. From Fig. 4, the result after Kalman filtering shows smoothness, low noise and fewer false peaks. The next step is to extract the gait parameters from the motion trajectory.
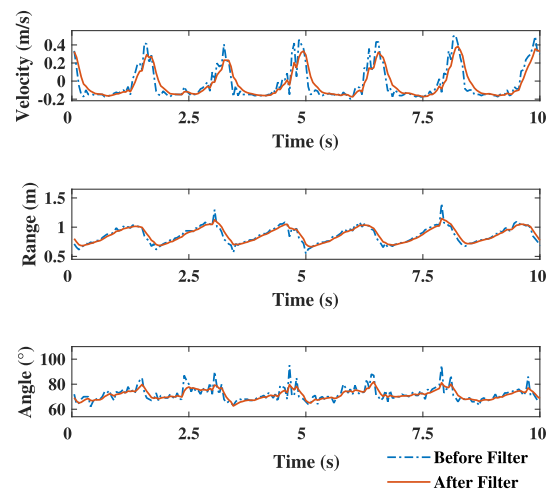


**FIGURE 4.** Example of velocity, range and angle measurements before and after applying the Kalman filter.

## B. EXTRACTION OF GAIT PARAMETERS

The gait cycle is defined as the time between the initial contact of the foot with the ground and the next occurrence of the same event in the same lower limb. A gait cycle consists of a stance phase and swing phase (Fig. 1). The stance phase lasts from the heel-stride event to the toe-off event and occupies 60% of the gait cycle. The swing phase lasts from a toe-off event to a heel-stride event. In this study, 6 gait parameters were measured from the received radar signal. The significance and definition of each gait parameter are discussed elsewhere [1]. The methods of calculating gait parameters using FMCW radar and IMU sensors are described as follows.

### 1) STRIDE TIME

The stride time is the total amount of time of one gait cycle and is defined as the time elapsed from one heel strike to the next heel strike of the same foot. The stride time describes the duration of a gait cycle. In the case of radar, when a subject is walking toward the radar, the heel strike can be the moment when the foot is closest to the radar, and toe off can be the moment when the foot is farthest from the radar. In the graph

of the measured range (Fig. 5), the heel strike is the trough of the measured range graph, and toe off is the peak of the measured range graph. The stride time can be measured by measuring the time interval from the heel strike to the next heel-strike event. Furthermore, in this study, FMCW radar can identify the side of each foot; that is, stride time can be measured from each foot.
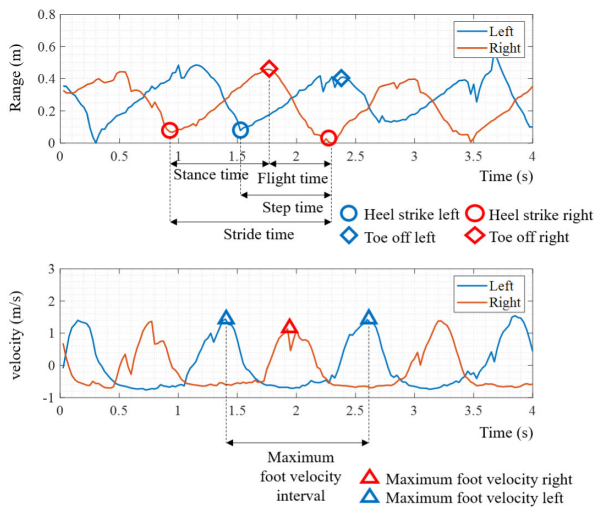


**FIGURE 5.** Range and velocity measurements of individual legs using FMCW radar.

### 2) STANCE TIME

The duration of stance time is the time interval during which the foot is in contact with the ground in a gait cycle. This means that the stance time is the time interval from heel strike to toe off. In this study, because the experiment was performed on a treadmill, the foot velocity was the same as the speed of the treadmill belt. The stance time can be measured from each of the left and right feet.

### 3) FLIGHT TIME

The flight time is the time interval while the foot is in the air. In contrast to the stance time, the flight time is the time interval from toe off to heel strike. The maximum speed appears during the flight time.

### 4) STEP TIME

The step time is the time interval from the moment one foot touches the floor to the moment the other foot touches the floor. From a radar point of view, the step time can be defined as the time interval from the heel strike of one foot to the heel strike of the other foot following in succession.

### 5) CADENCE

The cadence is defined as the number of steps per minute. For FMCW radar, the cadence can be calculated based on the number of stance times per minute. Based on [32], spontaneous cadence is usually between 98 and 138 steps/min for women and 91 and 135 steps/min for men, both applicable

to 18- to 49-year-olds. Women usually have a smaller step length and higher cadence.

### 6) MAXIMUM FOOT VELOCITY AND ITS INTERVAL

The foot velocity represents the overall performance of walking and is regarded as the sixth vital sign. It can be simply calculated as the product of step length and cadence. However, the FMCW radar has the capability of measuring velocity with high accuracy. The maximum foot velocity can be measured from the range-velocity map in every frame. In the velocity graph (Fig. 5), the local maximum value is the maximum foot velocity, and the interval between the peaks is the maximum foot velocity interval.

## IV. EXPERIMENTAL ENVIRONMENT
### A. SENSOR SETUP

The model name of the FMCW radar was an IWR6843ISK evaluation board from Texas Instruments with a data capture card DCA1000EVM board. The IWR6843ISK model is a millimeter wave sensor with a carrier frequency of 60 GHz used for industrial applications and has a 120° azimuth field of view (FOV) and 30° elevation FOV.

$$d_{res} = \frac{c}{2BW} \tag{15}$$

The bandwidth (BW) was set to 3.48 GHz, and the corresponding range resolution ($d_{res}$) was 4.31 cm (15). The maximum range ($d_{max}$) is proportional to the sampling rate ($f_s$) of the analog-to-digital converter (ADC) and inversely proportional to the chirp slope ($\mu$), so the maximum range was set to 5 meters (16). $c$ represents the speed of light (299792458 m/s). This range is sufficient to cover the experimental area and capture the gait motion on the treadmill.

$$d_{max} = \frac{f_s c}{2\mu} \tag{16}$$

The velocity resolution ($v_{res}$) is inversely proportional to the chirp time ($T_c$) and number of chirps ($N_c$). In this experiment, the chirp time was $35\mu sec$, and the number of chirps was 128; thus, the $v_{res}$ was 0.15 m/s (17). The number of frames per second (FPS) was set to 40.

$$v_{res} = \frac{\lambda}{2N_c T_c} \tag{17}$$

The FMCW module IWR6843ISK has 3tx and 4rx antennas, and among them, 2tx and 4rx were enabled to use MIMO antenna topology. By using TDM, 8 elements of the antenna array were configured as virtual antennas [33], [34]. The angle resolution of the array antenna ($\theta_{res}$) is inversely proportional to the number of antenna elements ($N_{an}$).

$$\theta_{res} = \frac{2}{N_{an}} \tag{18}$$

The number of antenna elements used was 8; therefore, the angle resolution was 15°. Because there is a time delay between the transmission time of each tx when applying TDM, a phase shift occurs due to the target's speed.

**TABLE 2.** FMCW radar features.

| | |
|---|---|
| FMCW chip set | TI IWR6843ISK |
| Operating frequency | 60 GHz |
| Sweep bandwidth | 3.48 GHz |
| ADC sampling rate | 2000 ksps |
| Transmission power | 12 dBm |
| RX noise figure | 12 dB |
| Chirp slope | 60 MHz/us |
| Number of chirps in a frame | 128 |
| Slow-time sampling frequency | 40 Hz |
| Number of TX | 2 |
| Number of RX | 4 |

**TABLE 3.** IMU sensor features.

| | |
|---|---|
| IMU chip set | EBIMU-9DOFV5 |
| Acceleration FPS | 100 Hz |
| Angular velocity vector FPS | 100 Hz |
| Absolute orientation FPS | 100 Hz |
| Acceleration range | $\pm$ 8 G |
| Angular velocity range | 2000 degree/s |



(a) Experimental setup of the treadmill and FMCW radar

(b) Placement of the IMU sensor and knee flexion with an adjustable orthosis for simulating asymmetric gait

**FIGURE 6.** Experimental setup of the treadmill and sensor configuration.

To compensate for the phase shift and measure the angle accurately, Doppler compensation was applied to the received signals [35].

The detailed parameter settings in this experiment are listed in Table 2 and Table 3. As shown in Fig. 6a, the radar was placed at the front of the treadmill at a 30-cm distance and at a 30-cm height from the floor. The height of the radar was chosen to avoid interference from the signals reflected by the hand or knee and to obtain the line of sight (LoS), as the height of the treadmill was 13 cm. A more detailed explanation of the radar height and angle is described in the next subsection. The radar measured the radial velocity ($v_{rad}$) of movement and velocity along the electromagnetic wave propagation direction.

IMU sensors have been used in several gait analysis techniques, such as monitoring postoperative gait abnormalities [36], fall detection [37], fall-related gait parameters measured on a treadmill and in daily life [38], the nature of the Parkinsonian gait [39], analysis of daily life characteristics of the elderly [40] and assessment of foot trajectory in humans when walking [4]. The model of the IMU sensor used in this study was EBIMU-9DOFV5, which is a 9-degree-of-freedom IMU sensor (E2BOX, Hanam-si, Gyeonggi-do, Republic of Korea). We collected data by connecting the sensors to MATLAB (MathWorks, New York, MA, USA) on a PC using a UART-to-USB converter board. The IMU sensors were attached to each ankle (lateral malleolus). The treadmill model used in this study was KSP-1201 (HOMETREKKING, Seoul, Republic of Korea). The speed of the treadmill was fixed at level 3 and level 6, and the velocities were 0.6 and 1.2 m/s, respectively.

## B. RADAR INSTALLATION

Fig. 6 shows the experimental setup, including FMCW and IMU sensor installation. The radar was installed at the front side of the treadmill, and IMU sensors were placed on the participant's ankle. The height of the radar in the experiment

was chosen to avoid interference from reflected signals by the knee or other body parts. Fig. 7 describes interference from other body parts at different radar heights with 180-cm-tall participants. In the range-Doppler heatmap obtained at a 30-cm radar height (Fig. 7a), the incident target signals were from each foot (Fig. 7b). At a 50-cm height (Fig. 7d), there was an additional signal reflected by the left or right knee (Fig. 7d). At a 70-cm height, there were additional signals reflected by the knee and both hands (Fig. 7f). The signals reflected by the feet were smaller than those reflected by the hands because they are located at the center of the main beam compared with the feet. FMCW radar could obtain LoS over the treadmill and avoid interference coming from body parts other than the feet at a 30-cm height.

The radar measurement accuracy according to the azimuth angle was also observed. Considering the angle resolution and beam pattern, the best option is for the radar to point directly at the participant; however, there could be minor changes during actual use, so it is important to check the tolerance. In Fig. 8, the quality of the range and velocity measurements of radar compared by the IMU sensor is described using the root mean square error (RMSE) (19).

$$RMSE = \sqrt{\frac{\sum_{n=1}^{N} \left(s_{f,n} - s_{i,n}\right)^2}{N}} \quad (19)$$

$s_{f,n}$ represents FMCW measurements, $s_{i,n}$ represents IMU measurements, and N represents the sample number of each signal. Because the sampling rate of IMU is faster than that of FMCW, IMU measurements are downconverted and then used to obtain RMSE. When the radar was at 90° (radar pointing directly at the subject), the RMSE of both range and velocity measurements was at the minimum, and as the angle decreased, the RMSE value increased. The RMSE of the range measurement hardly increased at 80° compared with 90°; however, as the angle decreased further, the RMSE

(a) Radar setup at a 30 cm height

(b) Range-Doppler heatmap at a 30 cm height

(c) Radar setup at a 50 cm height

(d) Range-Doppler heatmap at a 50 cm height

(e) Radar setup at a 70 cm height

(f) Range-Doppler heatmap at a 70 cm height
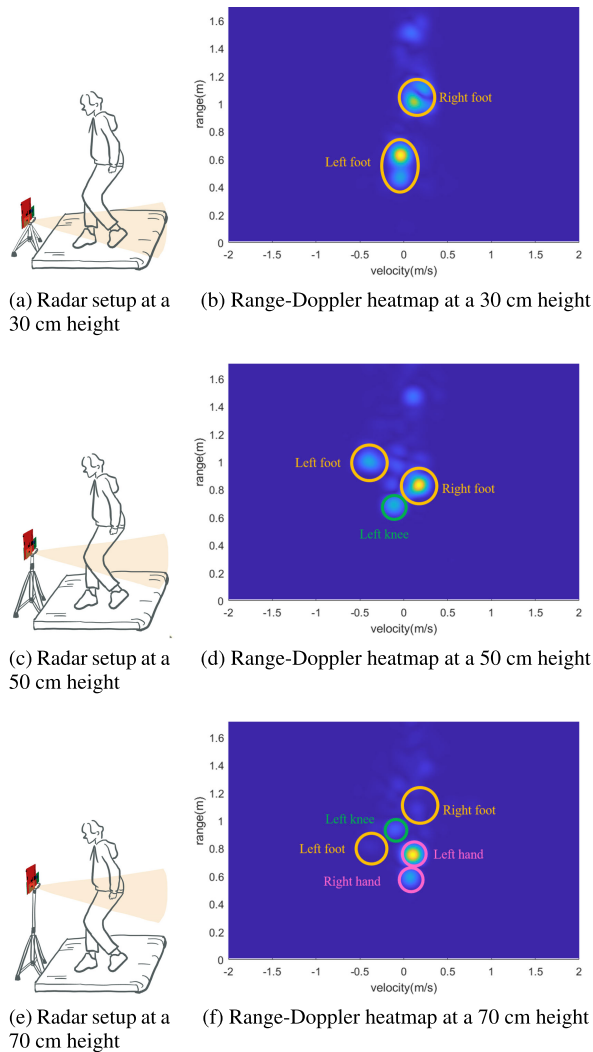
**FIGURE 7.** Range-doppler heatmap measured at different radar heights.



(a) The RMSE of range measurements according to the radar angle installation
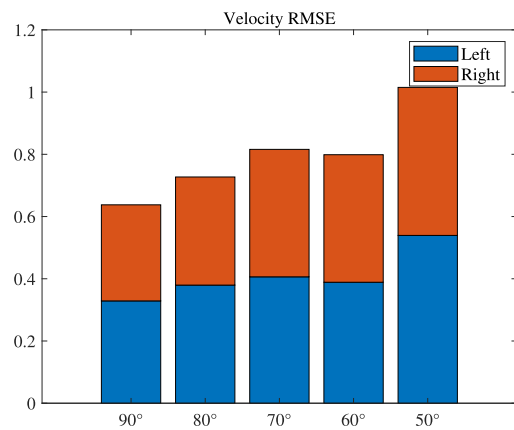
(b) The RMSE of velocity measurements according to the radar angle installation

**FIGURE 8.** RMSE of the range and velocity radar measurements against the IMU sensor according to the radar installation angle.

**TABLE 4.** Baseline characteristics.

|  | N=15 |
|---|---|
| Age (years) | 31.13 ± 6.85 |
| Sex (male) | 10 (66.66%) |
| Height (m) | 1.70 ± 0.06 |
| Weight (kg) | 69.60 ± 17.63 |
| Body mass index (kg/m$^2$) | 23.78 ± 5.05 |
| Stride time (s) | 1.16 ± 0.29 |
| Stance time (s) | 0.71 ± 0.21 |
| Flight time (s) | 0.45 ± 0.09 |
| Step time (s) | 0.57 ± 0.15 |
| Cadence (steps/s) | 50.74 ± 14.27 |
| Data are described as the mean ± SD or N(%) | |

increased considerably. For velocity measurement, the RMSE increment was not noticeable until 50°.

## C. BASELINE CHARACTERISTICS AND EXPERIMENTAL PROTOCOL

The experiment was conducted at Hanyang University, Seoul, South Korea. The Institutional Review Board of Hanyang University reviewed and approved the study protocols and monitored the study processes (IRB No. HYUIRB-202101-015). A total of 15 participants without any known diseases participated in the experiment. The participants' baseline characteristics are listed in Table 4. The average age of the participants was 31.1 years, and 66.6% of them were male. The average height, weight and body mass index (BMI) of the participants were 1.70 m, 69.60 kg and 23.78 kg/m$^2$, respectively. The average standard deviations of stride time, stance time, flight time, step time and cadence of participants were calculated using an IMU sensor.

People have their own speed of walking and running. Fig. 9 shows the range and velocity of each foot measured by

FMCW radar when the treadmill speed increased from level 1 (0.2 m/s) to 6 (1.2 m/s) and then decreased from level 6 to 1. From 0 to 15 seconds, the treadmill speed increased from level 1 to 6, and the treadmill speed then decreased to level 1. As the treadmill speed increased, the peak velocity of each foot also increased, and the feet moved faster. To perform the experiment, the treadmill speed was fixed to levels 3 and 6 as

representative speeds of walking and running, respectively, even though the proposed method could utilize a variety of ranges and speeds.
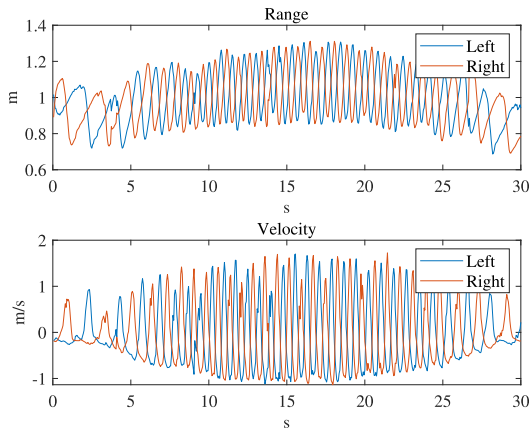


**FIGURE 9.** Range and velocity measurements with a speed change from level 1 to 6.

In the experiment, the participants were asked to walk on the treadmill while wearing IMU sensors on their ankles. In the experimental protocol, scenarios of walking at different velocities and those that can simulate asymmetry were included. The participants were asked to wear a knee orthosis when simulating gait asymmetry. Fig. 6b shows the placement of IMU sensors at the ankle (lateral malleolus) and the orthosis attached to the knee. In the experimental protocol, the participants were initially asked to walk on the treadmill for 1 minute at a fixed speed (0.6 m/s). Second, they were asked to run on the treadmill for 1 minute at a fixed speed (1.2 m/s). Third, they were asked to walk on the treadmill for 1 minute at a fixed speed (0.6 m/s) wearing a knee orthosis on their right leg. Finally, they were asked to walk on the treadmill for 1 minute at a fixed speed (0.6 m/s) wearing a knee orthosis on their left leg. The data were collected together with a time stamp and then synchronized.

### D. STATISTICAL ANALYSIS

Age, sex, height, weight, and body mass index were obtained from each participant, and gait parameters, including stride time, stance time, flight time, step length and step time, were obtained using an IMU sensor as baseline characteristics. Numerical data are presented as means $\pm$ SD, and categorical data including sex are presented as the number (%). The agreement of individual and averaged gait parameters measured using FMCW radar with those measured using the IMU sensor was evaluated using the intraclass correlation coefficient (ICC). Bland-Altman (BA) plots were generated to graphically present the amount of bias, and the levels of biases and limits of agreement (LOAs) were evaluated between the FMCW radar measurements and the IMU sensor measurements. The cutoff value for the gait asymmetry indicator (20) was decided using Youden's J index in the receiver operating characteristic (ROC) curve analysis. The diagnostic

**TABLE 5.** Computer specifications.

| CPU | Intel Core i9-9900K |
|---|---|
| RAM | 64GB |
| GPU | NVIDIA GeForce RTX 2070 SUPER |
| MATLAB ver. | R2019b |

performance of radar for gait asymmetry was evaluated. All statistical analyses were performed using MATLAB version 2019b. A *p*-value of $< 0.001$ was considered significant.

## V. RESULTS

The whole algorithm was run using a desktop computer, and its specifications are described in Table 5. Among the parts of the algorithm, the peak-finding part took the longest time, at 0.028 (29.4%) seconds per frame. The second most time-consuming part was the clutter-removing part, which took 0.022 (23.2%) seconds. The whole algorithm took 0.095 seconds per frame.

Fig. 10 shows a scatter plot and BA plot of individual gait parameters of each left and right leg from the FMCW radar and IMU sensors. Except for cadence, which was averaged over 1 minute, the maximum foot velocity interval (ICC 0.981 [confidence interval, CI 0.980-0.982]) and stride time (ICC 0.972 [CI 0.971-0.973]) showed the greatest level of agreement overall, and the square of the Pearson correlation coefficient $r^2$ was 0.96 and 0.95, respectively, which was close to 1. The mean bias between the FMCW radar and IMU sensor was zero. The individual stance time showed a high level of agreement (ICC 0.925 [CI 0.921-0.928]), although this agreement was relatively smaller than the agreement metrics for individual stride time and the maximum foot velocity interval. The $r^2$ was 0.87, and the mean bias between the FMCW radar and IMU sensor was 0.01. The individual flight time showed a relatively low level of agreement (ICC 0.648 [CI 0.633-0.663]); however, the mean and LOA width of bias measurements were similar to those of stride time and stance time. The $r^2$ was 0.44, and the mean bias between the FMCW radar and the IMU sensor was 0.01. The individual step time showed a good level of agreement (ICC 0.823 [CI 0.812-0.835]), $r^2$ was 0.69, and the mean bias between the FMCW radar and IMU sensor was 0.00. The cadence showed an excellent level of agreement (ICC 0.999 [CI 0.999-0.999]), $r^2$ was 1.00, and the mean bias between the FMCW radar and the IMU sensor was 0.08.

All the individual gait parameters showed similar LOA widths and mean biases, and the ICC value was relatively proportional to the amount of time spent in a single stride cycle. The cadence showed excellent agreement, as it is the number of steps averaged per minute. Table 6 shows the statistical values of all the individual and averaged gait parameters between FMCW radar and IMU sensors. Most of the gait parameters showed a great level of agreement except for the individual flight time, but the LOA width and mean bias were similar. All the parameters showed a greater level of agreement when averaged, and the LOA width decreased dramatically.

(a) Scatter plot and BA plot of stride time

(b) Scatter plot and BA plot of stance time

(c) Scatter plot and BA plot of flight time

(d) Scatter plot and BA plot of step time

(e) Scatter plot and BA plot of maximum foot velocity interval

(f) Scatter plot and BA plot of cadence
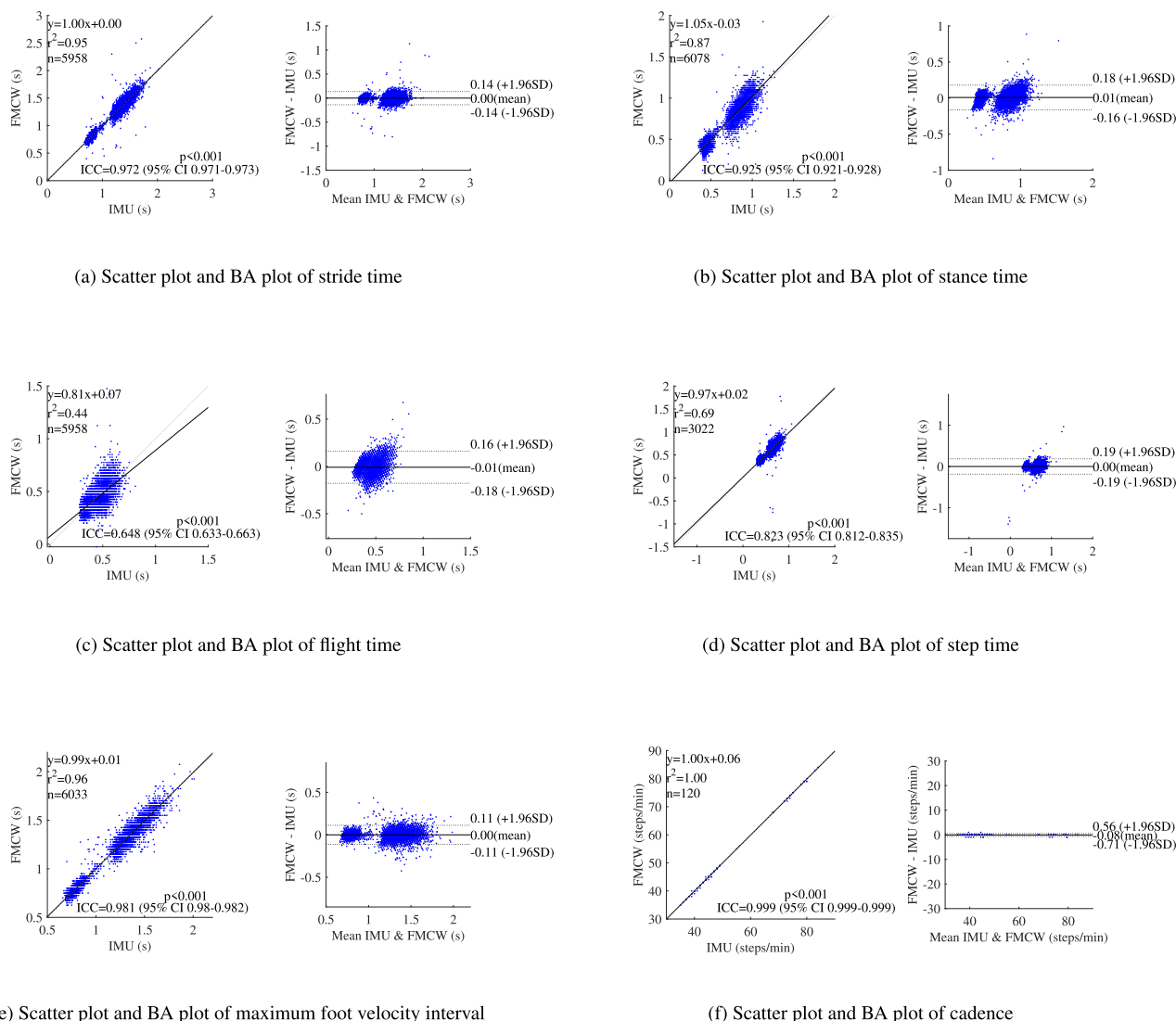
**FIGURE 10.** Scatter plot and BA plot of individual gait parameters using FMCW radar and IMU sensors.

**TABLE 6.** Agreement of gait parameters using FMCW and IMU sensors.

|  | ICC (95% CI) | Mean bias | Upper LOA | Lower LOA | *p*-value |
|---|---|---|---|---|---|
| Stride time | 0.972 (0.971-0.973) | 0.00 | 0.14 | -0.14 | <0.001 |
| Average stride time | 0.999 (0.999-0.999) | 0.00 | 0.00 | 0.00 | <0.001 |
| Stance time | 0.925 (0.921-0.928) | 0.01 | 0.18 | -0.16 | <0.001 |
| Average stance time | 0.975 (0.964-0.982) | 0.01 | 0.10 | -0.07 | <0.001 |
| Flight time | 0.648 (0.633-0.663) | -0.01 | 0.16 | -0.18 | <0.001 |
| Average flight time | 0.851 (0.794-0.894) | -0.01 | 0.07 | -0.1 | <0.001 |
| Step time | 0.823 (0.812-0.835) | 0.00 | 0.19 | -0.19 | <0.001 |
| Average step time | 0.955 (0.927-0.973) | 0.00 | 0.08 | -0.08 | <0.001 |
| Maximum foot velocity interval | 0.981 (0.980-0.982) | 0.00 | 0.11 | -0.11 | <0.001 |
| Average maximum foot velocity interval | 0.999 (0.999-0.999) | 0.00 | 0.00 | 0.00 | <0.001 |
| Cadence | 0.999 (0.999-0.999) | -0.08 | 0.56 | -0.71 | <0.001 |

ICC, intraclass correlation coefficient; LOA, limit of agreement; CI, confidence interval

Fig.11 describes the RMSE of gait parameters of individual participants except for the cadence, for which the ICC was 0.999 and very accurate. Among all the RMSEs, that of the 8th participant was especially large compared with those of the other participants because that participant was unaccustomed to that particular treadmill speed, which made his/her step awkward (Supplementary material). Compared with the other participants, the 8th participant had a large error, but it was still low compared with the gait parameter measurements in Table 4.
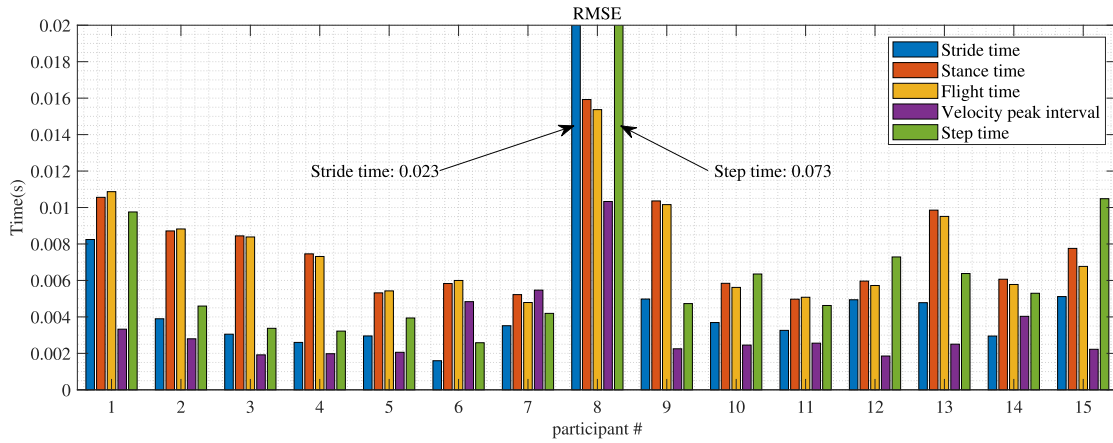
**FIGURE 11.** Bar graph of RMSE of each participant's gait parameters.
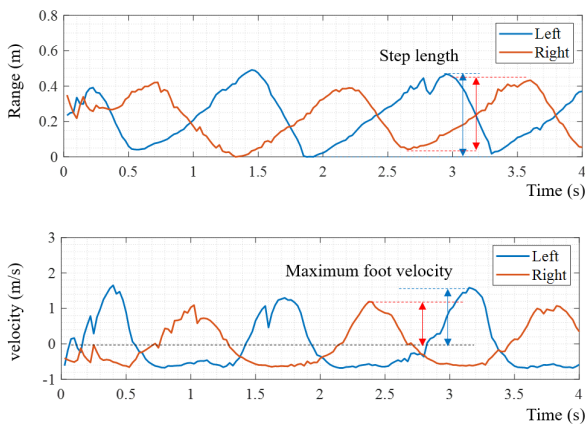


**FIGURE 12.** Range and velocity measured by FMCW radar while wearing a knee orthosis on the right leg.

**TABLE 7.** Recognition of gait asymmetry using FMCW radar.

| | | Ground truth | |
| --- | --- | --- | --- |
| | | Abnormal (N=30) | Normal (N=30) |
| Radar | Abnormal (N=25) | 25 | 0 |
| Cut-off value 0.178 | Normal (N=35) | 5 | 30 |
| | sensitivity=0.83, specificity=1.00, CCR=0.91 | | |

By observing the gait of the abnormal group, differences in maximum foot velocity and step length were captured. The leg side with the knee orthosis showed reduced step length and maximum foot velocity (Fig. 12). By using these factors, we proposed a parameter called the gait asymmetry indicator (GAI, (20)), which can detect and quantify the level of gait asymmetry.

$$GAI = | MFV_R / MFV_L - 1 | \qquad (20)$$

The ratios of peak velocity and step length for the right and left feet can indicate gait asymmetry. MFV represents maximum foot velocity, and the subscripts R and L represent
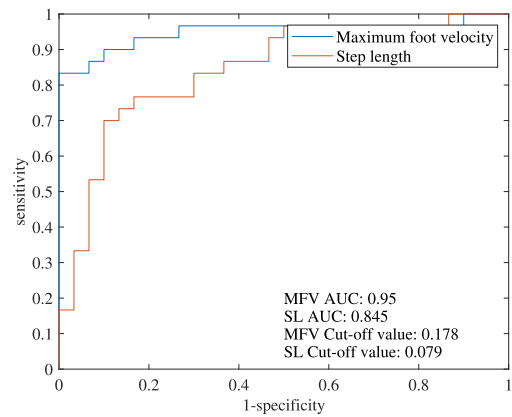


(a) ROC curve of maximum foot velocity and step length as a parameter with which to detect gait asymmetry.
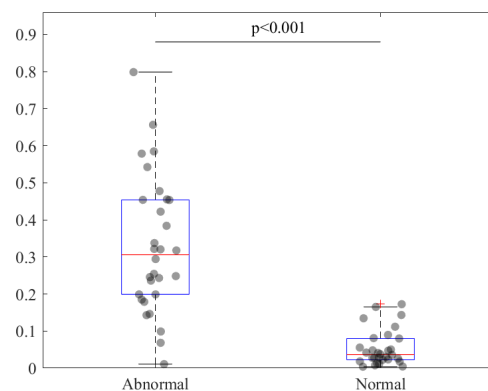


(b) Boxplots of GAI in the abnormal and normal groups.

**FIGURE 13.** Boxplot and ROC curve.

right and left, respectively. The greater the GAI is, the greater the level of gait asymmetry. Two gait parameters, maximum foot velocity and step length, were used for the GAI and evaluated using an ROC curve (Fig. 13a). The c-statistic of maximum foot velocity was 0.95, and that of step length was

0.845, which showed that using maximum foot velocity for GAI was better (Fig. 13a). The abnormal group showed a higher GAI than the normal group, as shown in Fig. 13b (median [interquartile range] of 0.30 [0.20-0.45] Hz vs. 0.03 [0.02-0.08] Hz, respectively; p < 0.01). Using maximum foot velocity as a GAI parameter showed a sensitivity of 0.83, a specificity of 1.00 and a correct classification rate of 0.91 at the 0.178 threshold set at the maximum value of Youden's J-point (Table 7).

## VI. CONCLUSION

In this paper, we proposed a new method of noncontact gait analysis using MIMO FMCW that can differentiate between the left and right foot. The received signals were preprocessed to obtain data on velocity, range, and angle, and those data were utilized and grouped to separate left and right feet. Then, gait parameters were calculated and compared with those measured by IMU sensors. To evaluate the accuracy of the algorithm, 15 participants were recruited and participated in the experiment. In the experimental protocol, the participants were asked to walk, run normally and walk with a knee orthosis on their left and right leg, respectively, on a treadmill. The correlation of gait parameters was high between the two sensors and was evaluated using scatter plots, BA plots, ICCs and other statistics. Moreover, we suggested a parameter, the GAI, that measures the ratio of gait parameters from the left and right feet to quantify the level of asymmetry of the left and right feet, respectively, and it could detect gait asymmetry with high accuracy. The gait analysis devices in use to date have been contact methods or are very expensive. Radar is being researched for gait analysis because it is a relatively inexpensive technology and can provide noncontact gait analysis. There have been several studies of noncontact gait analysis using CW and FMCW radar, but most of them could not measure gait parameters of the left and right side separately. This study shows that MIMO radar types can provide noncontact gait analysis in a more accurate and detailed manner. The limitation of this work is the absence of data from actual limping patients. However, simulated data using orthosis devices were obtained in this work, and the feasibility of MIMO FMCW radar to separate abnormal gaits was validated. In the next step, we plan to gather data from real patients by cooperating with medical doctors. In conclusion, MIMO FMCW radar offers a promising technology for gait analysis at home or in the clinic that can complement existing tools and aid healthcare professionals in early diagnosis and the course of treatment.

## REFERENCES

[1] A. Gouelle and F. Mégrot, "Interpreting spatiotemporal parameters, symmetry, and variability in clinical gait analysis," in *Handbook Human Motion*, B. Müller, S. I. Wolf, G.-P. Brueggemann, Z. Deng, A. McIntosh, F. Miller, and W. S. Selbie, Eds. Cham, Switzerland: Springer, 2016, pp. 1–20.

[2] G. V. Prateek, P. Mazzoni, G. M. Earhart, and A. Nehorai, "Gait cycle validation and segmentation using inertial sensors," *IEEE Trans. Biomed. Eng.*, vol. 67, no. 8, pp. 2132–2144, Aug. 2020.

[3] R. Kaur, Z. Chen, R. Motl, M. E. Hernandez, and R. Sowers, "Predicting multiple sclerosis from gait dynamics using an instrumented treadmill: A machine learning approach," *IEEE Trans. Biomed. Eng.*, vol. 68, no. 9, pp. 2666–2677, Sep. 2021.

[4] N. Kitagawa and N. Ogihara, "Estimation of foot trajectory during human walking by a wearable inertial measurement unit mounted to the foot," *Gait Posture*, vol. 45, pp. 110–114, Mar. 2016.

[5] L. S. Vargas-Valencia, A. Elias, E. Rocon, T. Bastos-Filho, and A. Frizera, "An IMU-to-body alignment method applied to human gait analysis," *Sensors*, vol. 16, no. 12, p. 2090, Dec. 2016.

[6] O. Postolache, J. M. D. Pereira, M. Ribeiro, and P. Girão, "Assistive smart sensing devices for gait rehabilitation monitoring," in *ICTs for Improving Patients Rehabilitation Research Techniques* (Communications in Computer and Information Science), H. M. Fardoun, V. M. R. Penichet, and D. M. Alghazzawi, Eds. Berlin, Germany: Springer, 2015, pp. 234–247.

[7] M. Nieto-Hidalgo, F. J. Ferrández-Pastor, R. J. Valdivieso-Sarabia, J. Mora-Pascual, and J. M. García-Chamizo, "A vision based proposal for classification of normal and abnormal gait using RGB camera," *J. Biomed. Inform.*, vol. 63, pp. 82–89, Oct. 2016.

[8] A.-K. Seifert, A. M. Zoubir, and M. G. Amin, "Detection of gait asymmetry using indoor Doppler radar," in *Proc. IEEE Radar Conf. (RadarConf)*, Apr. 2019, pp. 1–6.

[9] T.-N. Nguyen, H.-H. Huynh, and J. Meunier, "Human gait symmetry assessment using a depth camera and mirrors," *Comput. Biol. Med.*, vol. 101, pp. 174–183, Oct. 2018.

[10] J. W. Choi, X. Quan, and S. H. Cho, "Bi-directional passing people counting system based on IR-UWB radar sensors," *IEEE Internet Things J.*, vol. 5, no. 2, pp. 512–522, Apr. 2018.

[11] Y. Lee, J.-Y. Park, Y.-W. Choi, H.-K. Park, S.-H. Cho, S. H. Cho, and Y.-H. Lim, "A novel non-contact heart rate monitor using impulse-radio ultra-wideband (IR-UWB) radar technology," *Sci. Rep.*, vol. 8, no. 1, Dec. 2018, Art. no. 13053.

[12] Y. Zhang, X. Li, R. Qi, Z. Qi, and H. Zhu, "Harmonic multiple loop detection (HMLD) algorithm for not-contact vital sign monitoring based on ultra-wideband (UWB) radar," *IEEE Access*, vol. 8, pp. 38786–38793, 2020.

[13] S. Ahmed, D. Wang, J. Park, and S. H. Cho, "UWB-gestures, a public dataset of dynamic hand gestures acquired using impulse radar sensors," *Sci. Data*, vol. 8, no. 1, pp. 1–9, Dec. 2021.

[14] F. Khan, S. K. Leem, and S. H. Cho, "In-air continuous writing using UWB impulse radar sensors," *IEEE Access*, vol. 8, pp. 99302–99311, 2020.

[15] W. H. Lee, J. I. Kim, A. M. Kwon, J. H. Cha, D. Yim, Y.-H. Lim, S.-H. Cho, S. H. Cho, and H.-K. Park, "Quantified assessment of hyperactivity in ADHD youth using IR-UWB radar," *Sci. Rep.*, vol. 11, no. 1, pp. 1–10, Dec. 2021.

[16] J. Li, S. L. Phung, F. H. C. Tivive, and A. Bouzerdoum, "Automatic classification of human motions using Doppler radar," in *Proc. Int. Joint Conf. Neural Netw. (IJCNN)*, Jun. 2012, pp. 1–6.

[17] F. Wang, M. Skubic, M. Rantz, and P. E. Cuddihy, "Quantitative gait measurement with pulse-doppler radar for passive in-home gait assessment," *IEEE Trans. Biomed. Eng.*, vol. 61, no. 9, pp. 2434–2443, Sep. 2014.

[18] Z. Chen, G. Li, F. Fioranelli, and H. Griffiths, "Personnel recognition and gait classification based on multistatic micro-Doppler signatures using deep convolutional neural networks," *IEEE Geosci. Remote Sens. Lett.*, vol. 15, no. 5, pp. 669–673, May 2018.

[19] Z. Ni and B. Huang, "Human identification based on natural gait micro-Doppler signatures using deep transfer learning," *IET Radar, Sonar Navigat.*, vol. 14, no. 10, pp. 1640–1646, Oct. 2020.

[20] D. P. LaRoche, S. B. Cook, and K. Mackala, "Strength asymmetry increases gait asymmetry and variability in older women," *Med. Sci. Sports. Exerc.*, vol. 44, no. 11, pp. 2172–2181, Nov. 2012.

[21] I. Bautmans, B. Jansen, B. Van Keymolen, and T. Mets, "Reliability and clinical correlates of 3D-accelerometry based gait analysis outcomes according to age and fall-risk," *Gait Posture*, vol. 33, no. 3, pp. 366–372, Mar. 2011.

[22] T. Ramakrishnan, C.-A. Lahiff, and K. B. Reed, "Comparing gait with multiple physical asymmetries using consolidated metrics," *Frontiers Neurorobotics*, vol. 12, p. 2, Feb. 2018.

[23] G. Yogev, M. Plotnik, C. Peretz, N. Giladi, and J. M. Hausdorff, "Gait asymmetry in patients with Parkinson's disease and elderly fallers: When does the bilateral coordination of gait require attention?" *Exp. Brain Res.*, vol. 177, no. 3, pp. 336–346, Mar. 2007.

[24] L. De Vito, O. Postolache, and S. Rapuano, "Measurements and sensors for motion tracking in motor rehabilitation," *IEEE Instrum. Meas. Mag.*, vol. 17, no. 3, pp. 30–38, Jun. 2014.

[25] A. R. Anwary, H. Yu, and M. Vassallo, "Optimal foot location for placing wearable IMU sensors and automatic feature extraction for gait analysis," *IEEE Sensors J.*, vol. 18, no. 6, pp. 2555–2567, Mar. 2018.

[26] S. Kim, D. Oh, and J. Lee, "Joint DFT-ESPRIT estimation for TOA and DOA in vehicle FMCW radars," *IEEE Antennas Wireless Propag. Lett.*, vol. 14, pp. 1710–1713, 2015.

[27] S. Saponara and B. Neri, "Radar sensor signal acquisition and multidimensional FFT processing for surveillance applications in transport systems," *IEEE Trans. Instrum. Meas.*, vol. 66, no. 4, pp. 604–615, Apr. 2017.

[28] *Find Local Maxima MATLAB Findpeaks*. [Online]. Available: https://www.mathworks.com/help/signal/ref/findpeaks.html

[29] S. N. Kadir, D. F. M. Goodman, and K. D. Harris, "High-dimensional cluster analysis with the masked EM algorithm," *Neural Comput.*, vol. 26, no. 11, pp. 2379–2394, Nov. 2014.

[30] M.-S. Yang, C.-Y. Lai, and C.-Y. Lin, "A robust EM clustering algorithm for Gaussian mixture models," *Pattern Recognit.*, vol. 45, no. 11, pp. 3950–3961, 2012.

[31] G. Welch and G. Bishop, *An Introduction to the Kalman Filter*. Chapel Hill, NC, USA, 1995.

[32] D. Levine, J. Richards, and M. W. Whittle, *Whittle's Gait Analysis*. Amsterdam, The Netherlands: Elsevier, 2014.

[33] A. Ahmad, J. C. Roh, D. Wang, and A. Dubey, "Vital signs monitoring of multiple people using a FMCW millimeter-wave sensor," in *Proc. IEEE Radar Conf.*, Oklahoma City, OK, USA, Apr. 2018, pp. 1450–1455.

[34] B. Li, J. Zhang, Y. Deng, Z. Zhou, and L. Sun, "Design of two-dimensional millimeter wave virtual array based on sparse MIMO array," in *Proc. Photon. Electromagn. Res. Symp. Fall (PIERS-Fall)*, Dec. 2019, pp. 2240–2244.

[35] C. M. Schmid, R. Feger, C. Pfeffer, and A. Stelzer, "Motion compensation and efficient array design for TDMA FMCW MIMO radar systems," in *Proc. 6th Eur. Conf. Antennas Propag. (EUCAP)*, Mar. 2012, pp. 1746–1750.

[36] R. Hanly, F. Doyle, S. Whitehouse, and A. Timperley, "Outpatient 3-D gait analysis one year after THA using a portable IMU system," *Orthopaedic Proc.*, vol. 98-B, p. 1, Jun. 2016.

[37] N. Shibuya, B. T. Nukala, A. I. Rodriguez, J. Tsay, T. Q. Nguyen, S. Zupancic, and D. Y. C. Lie, "A real-time fall detection system using a wearable gait analysis sensor and a support vector machine (SVM) classifier," in *Proc. ICMU*, Jan. 2015, pp. 66–67.

[38] S. M. Rispens, J. H. Van Dieën, K. S. Van Schooten, L. E. Cofré Lizama, A. Daffertshofer, P. J. Beek, and M. Pijnappels, "Fall-related gait characteristics on the treadmill and in daily life," *J. NeuroEng. Rehabil.*, vol. 13, no. 1, p. 12, Feb. 2016.

[39] S. Okuda, S. Takano, M. Ueno, Y. Hara, Y. Chida, T. Ikkaku, F. Kanda, and T. Toda, "Gait analysis of patients with Parkinson's disease using a portable triaxial accelerometer," *Neurol. Clin. Neurosci.*, vol. 4, no. 3, pp. 93–97, 2016.

[40] S. A. Fouaz, H. P. Nguyen, C. Lavigne-Pelletier, E. Goubault, P. Boissy, and C. Duva, "Wavelet-based algorithm for auto-detection of daily living activities of older adults captured by multiple inertial measurement units (IMUs)," *Physiol. Meas.*, vol. 37, no. 3, p. 442, 2016.

**DINGYANG WANG** (Student Member, IEEE) received the B.S. degree in electronic engineering from Andong National University, Gyeongsangbuk-do, South Korea, in 2015. He is currently pursuing the joint M.S. and Ph.D. degrees in electronic engineering with Hanyang University, Seoul, South Korea. His research interests include signal processing and embedded implementation, especially regarding detection, vital signs, and gait analysis and imaging using IR-UWB and FMCW radar.

**JUNYOUNG PARK** (Student Member, IEEE) received the B.S. and M.S. degrees in electronic engineering from Hanyang University, Seoul, South Korea, in 2016 and 2018, respectively, where he is currently pursuing the Ph.D. degree. His research interests include signal processing and embedded implementation, especially regarding detection, vital signs, and gait analysis and imaging using IR-UWB and FMCW radar.

**HEE-JIN KIM** received the M.D. and Ph.D. degrees from Hanyang University, Seoul, South Korea. She is currently a Professor with the Neurology Department, College of Medicine, Hanyang University. She worked as a Clinical Fellow with Konkuk University, from 2006 to 2008, and started work as a Clinical Assistant Professor with Hanyang University's Neurology Department, in 2008. She was promoted to an Assistant Professor and an Associate Professor, in 2012 and 2015, respectively. She worked as an Associate Professor with the Department of Psychiatry, Center for Brain Health, New York University, with Mony John de Leon, who is a Renowned Scholar in the neuroimaging of dementia, from 2015 to 2016. She is currently the Director of the Center for Cognition and Brain Health. Her research interests include pathomechanisms and pharmacological interventions for neurodegenerative diseases, including dementia neuroimaging.
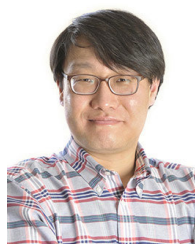
**KOUNSEOK LEE** received the degree from the College of Medicine, Hanyang University, Seoul, South Korea, in 2005, the M.D. degree from Hanyang University Medical Center, and the Ph.D. degree in psychiatry from Hanyang University. He is currently a Clinical Assistant Professor with Hanyang University Medical Center. He is also a Research Assistant Professor with Hanyang University, where he completed a residency in psychiatry. He obtained membership in the Korean Board of Psychiatry, in 2010. He completed a bipolar disorder and schizophrenia fellowship at Samsung Medical Center between 2013 and 2015. He and his collaborators are developing detection methods to investigate the risk factors for suicide and mood disorders. The goal of his work is to develop a clearer understanding of suicide and develop treatments.

**SUNG HO CHO** (Member, IEEE) received the Ph.D. degree in electrical and computer engineering from The University of Utah, Salt Lake City, USA, in 1989. From 1989 to 1992, he was a Senior Member of the technical staff with the Electronics and Telecommunications Research Institute, Daejon, South Korea. He joined the Department of Electronic Engineering, Hanyang University, Seoul, South Korea, in 1992, where he is currently a Professor. His research interests include applied signal processing, machine learning, radar computing, digital healthcare for signal processing, context-aware computing, radar sensors, smart space, and wireless networks.

• • •